Journal of Inorganic Biochemistry 146 (2015) 69–76

Contents lists available at ScienceDirect

Journal of Inorganic Biochemistry

journal homepage: www.elsevier.com/locate/jinorgbio

A new mononuclear manganese(III) complex of an unsymmetrical hexadentate N_3O_3 ligand exhibiting superoxide dismutase and catalase-like activity: synthesis, characterization, properties and kinetics studies

Gabriela N. Ledesma [a], Hélène Eury [b,c], Elodie Anxolabéhère-Mallart [d], Christelle Hureau [b,c], Sandra R. Signorella [a,*]

[a] IQUIR (Instituto de Química Rosario), Consejo Nacional de Investigaciones Científicas y Técnicas (CONICET), Facultad de Ciencias Bioquímicas y Farmacéuticas, Universidad Nacional de Rosario, Suipacha 531, (S2002LRK), Rosario, Argentina
[b] Laboratoire de Chimie de Coordination, UPR CNRS 8241, 205 Route de Narbonne, 31077 Toulouse Cedex 04, France
[c] Université de Toulouse; UPS, INPT, LCC, F-31077 Toulouse, France
[d] Laboratoire d'Electrochimie Moléculaire UMR CNRS-P7 7591 Université Paris Diderot-Paris, 15 rue Jean-Antoine de Baïf, 75205 Paris Cedex 13, France

ARTICLE INFO

Article history:
Received 15 December 2014
Received in revised form 20 February 2015
Accepted 20 February 2015
Available online 2 March 2015

Keywords:
Mn complex
SOD/catalase activity
Kinetics
Mn-based ROS scavenger

ABSTRACT

A mononuclear Mn^{III} complex MnL·4H_2O (H_3L = 1-[N-(2-pyridylmethyl),*N*-(2-hydroxybenzyl)amino]-3-[*N*′-(2-hydroxybenzyl),*N*′-(4-methylbenzyl)amino]propan-2-ol) has been prepared and characterized. This complex catalyzes the dismutation of superoxide efficiently, with catalytic rate constant $k_{cat} = 1.7 \times 10^6\ M^{-1}\ s^{-1}$ and IC_{50} 1.26 μM, obtained through the nitro blue tetrazolium photoreduction inhibition superoxide dismutase assay, in aqueous solution of pH 7.8. MnL is also able to disproportionate more than 300 equivalents of H_2O_2 in CH_3CN, with initial rate of H_2O_2 decomposition given by $r_i = k_{cat}\,[MnL]^2\,[H_2O_2]$ and $k_{cat} = 1.32(2)\ mM^{-2}\ min^{-1}$. The accessibility of the Mn^{IV} state ($E^p = 0.53$ V vs. saturated calomel electrode), suggests MnL employs a high-valent catalytic cycle to decompose $O_2^{\bullet -}$ and H_2O_2.

1. Introduction

One of the major biological roles of Mn is related to oxygen metabolism, as the cofactor for antioxidant defense enzymes, which results from its unrivaled repertoire of redox chemistry [1]. The number and type of ligands, the local charge and nuclearity are among the factors that introduce a way of tuning the redox potential of the metal center to face electron transfer reactions. This redox function of Mn is reflected in the active site of specialized enzyme systems such as manganese catalases (MnCATs) and superoxide dismutases (MnSODs) that serve as the frontline molecular defense against H_2O_2 and $O_2^{\bullet -}$ in a number of organisms [2,3]. MnCAT enzymes share an unusual bridged binuclear manganese cluster that serves as the active site to perform the efficient two-electron disproportionation of H_2O_2 [2], whereas in MnSODs, the active site contains one pentacoordinate Mn ion in a N_3O_2 environment [3,4], interconverting between the reduced Mn^{II} and oxidized Mn^{III} states during turnover.

Due to the potential use as catalytic reactive oxygen species (ROS) scavengers for preventing oxidative stress injuries, numerous and diverse Mn compounds exhibiting SOD- or CAT-like activity have been reported [5,6]. Among them, several complexes have been reported to have dual SOD/CAT activity [7–15], an advantageous property since cytotoxic H_2O_2 is produced during $O_2^{\bullet -}$ disproportionation. Thus, catalase activity would be a key attribute for synthetic ROS scavenging compounds. The intrinsic dinuclear nature of the MnCAT active site has stimulated activity studies on complexes of binucleating ligands which provide an internal bridge to stabilize the dimanganese unit [6,16]. However, a number of mononuclear Mn complexes have shown CAT activity, for which efficiency seems to be related to the presence of at least one labile coordination position on the Mn ion [7–15,17–19]. This kind of mononuclear catalytic antioxidants has been proposed to react through a mechanism involving mononuclear $Mn^V = O$ species [20,21] or through formation of dimeric species in solution [22]. Mononuclear Mn complexes with the six coordination sites of the metal occupied by donor sites of the ligand constitute exceptional cases also exhibiting CAT activity [23], for which little is known. This has motivated our interest for gaining insights into the catalysis of H_2O_2 and $O_2^{\bullet -}$ disproportionation by mononuclear Mn^{III} complexes with six donor sites of the

* Corresponding author. Tel.: +54 341 4350214; fax: +54 341 4370477.
E-mail address: signorella@iquir-conicet.gov.ar (S.R. Signorella).

http://dx.doi.org/10.1016/j.jinorgbio.2015.02.012
0162-0134/

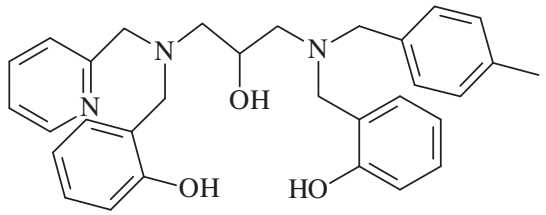

H_3L

Scheme 1. Ligand used in this work.

ligand in the coordination sphere. With this aim, we report here the synthesis, characterization, properties and SOD/CAT activity of a new mononuclear Mn^{III} complex obtained with the hexadentate N_3O_3 ligand 1-[*N*-(2-pyridylmethyl),*N*-(2-hydroxybenzyl)amino]-3-[*N′*-(2-hydroxybenzyl),*N′*-(4-methylbenzyl)amino]propan-2-ol (H_3L, Scheme 1) [24] and compare its catalytic activity with that of other mononuclear manganese catalysts.

2. Experimental section

2.1. Materials

All reagents were used as purchased without further purification. Solvents were purified by the standard methods. Ligand H_3L was obtained according to a recently described synthetic route [24].

2.2. Physical methods

Infrared spectra were recorded on a Perkin-Elmer Spectrum One FT-IR spectrophotometer. ESI (electrospray ionization)-mass spectra were carried out with a Bruker micrOTOF-Q II spectrometer, employing ~10^{-5} M solution of the complex, in acetonitrile or methanol. Optical spectra were recorded on a Jasco V-550 UV-visible (UV–vis) spectrophotometer with thermostated cell compartments. Melting point was taken on a Fisher–Johns (Ionomex) apparatus. EPR data were recorded using an Elexsys E 500 Bruker spectrometer, operating at a microwave frequency of approximately 9.5 GHz. Spectra were recorded using a microwave power of 0.5 mW (under nonsaturating conditions) with a modulation amplitude of 0.5 mT. Conductivity measurements were performed using a Horiba F-54 BW conductivity meter on 1.0 mM solutions of the complex in water. Magnetic susceptibility data were collected with a Quantum Design MPMS SQUID susceptometer. Cyclic voltammetry was recorded with an Autolab PGSTAT20 potentiostat. The counter electrode was a Pt wire, the reference electrode was a calomel electrode isolated in a fritted bridge, and the working electrode was a glassy carbon disk (diameter = 3 mm). Studies were carried out under Ar, in dry acetonitrile (ACROS) using 0.1 M tetrabutylammonium hexafluorophosphate ($TBAPF_6$) as a supporting electrolyte. Temperature was regulated with a Julabo circulation bath. The working electrode was carefully polished before each voltammogram with a 1 μm diamond paste, sonicated in an ethanol bath, washed with ethanol, and dried with compressed air. The ^1H and ^{13}C NMR spectra were acquired with a Bruker Avance spectrometer (300.13 and 75.48 MHz for ^1H and ^{13}C, respectively). ^1H spectra in the 90 to −30 ppm region were observed with a π/2 pulse preceded by pre-saturation of the water signal, on a spectral window of ca. 59 kHz, and with a total recycle time of ca. 30 ms. For the observation of signal at ca. 145 ppm, ^1H spectrum was acquired with a SuperWEFT pulse sequence on a spectral window of ca. 180 kHz. The chemical shifts (δ) are reported in ppm from internal TMS or residual solvent resonances. All spectra were recorded at 298 K.

2.3. Synthesis of complex $MnL{\cdot}4H_2O$

Triethylamine (32 μL, 0.23 mmol) and $MnCl_2{\cdot}4H_2O$ (0.015 g, 0.075 mmol) were added to a solution of H_3L (0.037 g, 0.075 mmol) in methanol (2.0 mL) with constant stirring. The color of the solution changed immediately and after 2 h at ambient temperature, the volume was reduced to aprox. 1 mL. The resulting microcrystalline deep brown powder was filtered, washed with cold diethyl ether and dried under vacuum. Recrystallization from acetonitrile afforded 0.030 g (0.048 mmol, 64%) of the complex. m.p.: 163–166 °C. ESI-MS: found m/z = 550.1871 [$MnLH^+$]; $C_{31}H_{33}MnN_3O_3$ requires m/z 549.1824. Anal. calcd. for $C_{31}H_{32}MnN_3O_3{\cdot}4H_2O$: C, 59.9; H, 6.5; Mn, 8.8; N, 6.8%; found C, 59.4; H, 5.2; Mn, 8.2; and N 7.2%. Although the analysis result for H is somewhat unsatisfactory, the chemical formula is consistent with the NMR, IR, magnetic, conductivity and mass spectrometry data. Significant IR bands (ATR (attenuated total reflectance), ν cm^{-1}): 3340, 2920, 1624, 1596, 1575, 1477, 1445, 1267, 1150, 1112, 1035, 1016, 882, 840, 754, 680, and 635. UV–vis λ_{max} nm (ε M^{-1} cm^{-1}) in CH_3CN: 211 (29900), 255 (sh, 16675); 356 (sh, 3796); and 490 (1241); in CH_3OH: 215 (21800); 256 (17525); 380 (3080); and 495 (1170).

2.4. Evaluation of CAT activity

The catalase-like activity of MnL was tested by volumetric determination of molecular oxygen that evolved after the addition of H_2O_2 to a solution of the complex in acetonitrile. A vial flask capped with a rubber septum, containing a degassed solution of the complex, was thermostated at 20 °C and connected through a cannula to a gas-measuring buret (precision of 0.1 mL). A solution of H_2O_2 ([H_2O_2]:[complex] ratio in the range 100–350:1; [complex] = 0.3–0.9 mM) was injected through the septum to the stirred complex solution, and the resulting volume of oxygen was measured with the buret.

2.5. SOD indirect assay

The SOD activity of the complexes was assayed by measuring the inhibition of the photoreduction of nitro blue tetrazolium (NBT), by a method slightly modified from that originally described by Beauchamps and Fridovich [25]. The solutions containing riboflavin (3.3×10^{-6} M), methionine (9.5×10^{-3} M), NBT (3.6×10^{-5} M) and the complex of various concentrations were prepared with phosphate buffer (pH 7.8). The mixtures were illuminated by a fluorescent lamp with a constant light intensity at 25 °C. The reduction of NBT was monitored at 560 nm with various illumination periods (t). Rates in the absence and in the presence of different concentrations of complex were determined and plotted vs. complex concentration. Inhibition percentage was calculated according to: $\{(\Delta Abs/t)_{\text{without complex}} - (\Delta Abs/t)_{\text{with complex}}\} \times 100/(\Delta Abs/t)_{\text{without complex}}$. The IC_{50} value represents the concentration of the SOD mimic that induces a 50% inhibition of the reduction of NBT. Control experiments were performed on mixtures of NBT + complex, riboflavin + complex, and NBT + methionine + complex, in phosphate buffer, to ensure that the complex does not react independently with any of the components of the mixture. The complex stability in the aqueous buffer was checked by UV–vis spectroscopy. Spectra of the complex registered at different time–lengths after preparation of the solution were identical (Fig. S1).

3. Results and discussion

3.1. Synthesis and spectroscopic characterization

Complex MnL was synthesized by treatment of a methanolic solution of H_3L with three equiv of triethylamine and one equiv of $MnCl_2$. Complexation occurs immediately after mixing the Mn^{II} salt with the deprotonated ligand, as evidenced by the observed change of color of

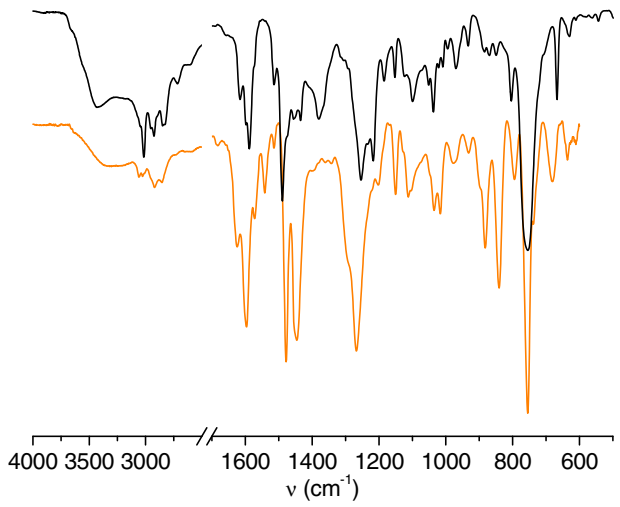

Fig. 1. FT-IR spectra of free ligand (black line, top) and MnL (orange line, bottom).

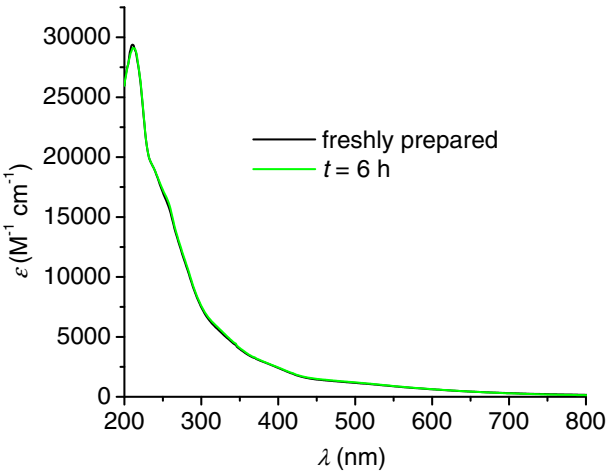

Fig. 3. Electronic spectrum of 0.123 mM MnL in CH_3CN. $T = 293$ K.

the reaction mixture from pale yellow to brown. Addition of base is required to facilitate formation of Mn^{III} and deprotonation of the ligand for coordination to the metal. The solid complex is air stable, non-hygroscopic, melts at 165 °C without decomposition, and has a room temperature magnetic moment of 4.9 BM, as expected for a high-spin octahedral Mn^{III} complex. The conductivity data for this compound in methanol show non-electrolytic behavior in this solvent (same conductivity as for the neat solvent), indicating that the complex is neutral in solution. Analytical results, magnetic and conductivity measurements point to a neutral complex of formula $Mn^{III}L$. This result evidences the versatility of L^{3-}, which in basic methanol, when higher metal to ligand ratio is used, yields a trinuclear Mn complex with 3:2 Mn to ligand ratio [26].

The IR spectrum of MnL shows the typical pattern of the deprotonated ligand L^{3-} bound to the Mn ion (Fig. 1). Intense phenolato and pyridyl absorptions are observed between 1624 and 1575 cm^{-1}, which are shifted by ≈ 8 and 13 cm^{-1}, respectively, from those in the free ligand because of the coordination of the metal to these groups. The peak at 1375 cm^{-1}, assigned to O–H in plane bending vibration of the phenol groups in the free ligand, is absent in the spectrum of the complex, indicating that deprotonated phenol groups are bound to manganese. Furthermore, the broad band at ~ 3340 cm^{-1} can be assigned to non-coordinated water molecules. Relevant IR vibration frequencies for H_3L and MnL are listed in Table S1.

The positive mode ESI-mass spectrum of the complex in CH_3CN (Fig. 2) shows peaks at m/z 572.2 and 550.2 originated from $[MnLNa]^+$ and $[MnLH]^+$ monocations, thus confirming its chemical composition. Other minor peaks at m/z 467.1 and 761.1 can be assigned to the fragment $[MnLNa–C_7H_6O]^+$ and the aggregate $[MnLH + N_2C_{14}H_{15}]^+$, respectively. A similar ESI-mass spectrum is observed in CH_3OH (Fig. S2). Other peaks at higher m/z are most likely to be generated during electrospray.

The electronic spectra of MnL recorded in CH_3CN and CH_3OH exhibit intense absorptions at 210–240 nm, attributed to $\pi \rightarrow \pi^*$ intraligand transitions and several ligand-to metal charge transfer (LMCT) transitions from the phenoxo to Mn^{III} in the region 300–500 nm, also observed for a variety of Mn^{III} complexes with phenoxo ligands (Fig. 3 and S3) [27–30]. The LMCT band at ~500 nm overlaps the *d–d* transitions that are observed as a tail (Fig. S4). In the two solvents, spectra of the complex registered at different times after preparation of solutions showed identical λ_{max} and molar absorbance coefficients, indicating that the complex is stable in these solvents.

^{13}C NMR spectroscopy was used as a way to establish the metal binding to donor sites of the ligand by analyzing the effect of addition of increasing amounts of $MnCl_2$ on the carbon chemical shifts of the deprotonated ligand in basic CD_3OD. Resonances of the ligand + NaOD in CD_3OD were assigned from the $^1H–^{13}C$ HSQC spectrum (Fig. S5). Upon addition of 0.1 to 1.0 equiv. of $MnCl_2$ to the basic CD_3OD solution of L^{3-} significant changes were observed (Fig. S6). Resonances ascribed to C_{ph}–OH and *C*H–OH are significantly more affected than any other. These signals show large broadening and are no longer observed after addition of 0.1 (HO–C_{ph}) and 0.25 equiv. (HO–*C*H—, C2 in Fig. S7) of salt, respectively. NMR spectra also showed broadening and moderate but significant up-field shifts of the ^{13}C nuclei adjacent to the N_{py} metal binding site (C8 and C12 in Fig. S7). Besides, signals assigned to the six –CH_2–N methylene groups suffered both broadening

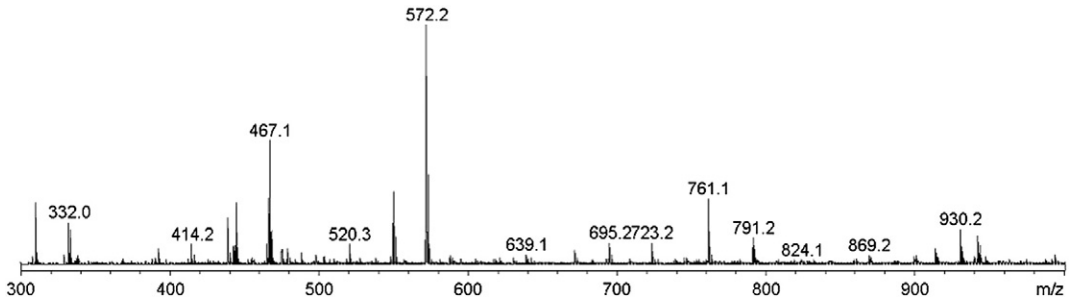

Fig. 2. ESI-Mass spectrum of MnL in CH_3CN.

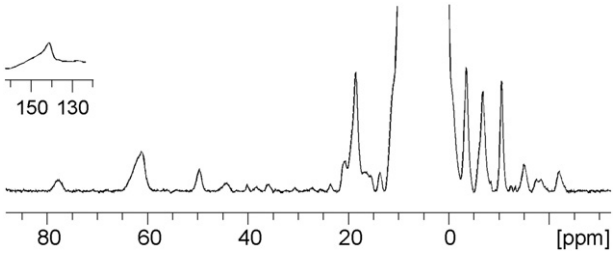

Fig. 4. ^{1}H NMR spectrum of L^{3-} (0.13 M) after the addition of 1.0 equiv of $MnCl_2$, in CD_3OD.

and chemical shift displacement from the values observed for the free ligand, and were no longer observed in the spectrum of the 1:1 metal to ligand mixture (C1, C3–C7 in Fig. S7). ^{13}C nuclei adjacent to the phenolato donor site showed broadening and up-field shift perturbation (C13, C19 in Fig. S7). The spectrum of the 1:1 ligand:metal mixture is dominated by resonances of the ^{13}C nuclei belonging to the tolyl moiety, the only ligand fragment not involved in metal coordination. These data support the metal complexation through the N_3O_3-donor sites of the ligand.

Paramagnetic ^{1}H NMR of deprotonated ligand/metal mixture in CD_3OD confirms phenolato and pyridine groups are involved in metal coordination. ^{1}H NMR spectrum for the 1:1 ligand:metal mixture is displayed in Fig. 4. The spectrum shows signals ranging from +147 to −23 ppm, with the envelope of diamagnetic signals between 0 and 12 ppm. The more intense resonances belong to the terminal pyridyl and phenolato ring protons, shifted down- or up-field depending on the dominating, σ or π, spin-delocalization. The spectrum of the 1:1 deprotonated ligand/metal mixture shows all peaks expected for the pyridyl and phenolato protons of MnL (although we have not attempted to assign them) as well as the broader peaks of methylene protons spanning the full range of the spectra [31].

3.2. Electrochemical studies

Cyclic voltammetry of MnL complex was studied at a glassy carbon, in CH_3CN solution (Fig. 5 and S8). The MnL complex was prepared in situ upon the addition of 1 mM of $Mn(ClO_4)_2.6H_2O$ to a 1 mM solution of H_3L in the presence of 3 equivalents of 2,6 dimethylpyridine (lutidine). Cyclic voltammogram of H_3L before the addition of Mn salt and base exhibits a series of intense and slightly irreversible waves at 0.9, 1.06 and 1.23 V vs. SCE (saturated calomel electrode) attributed to the oxidation of the phenol, the alcohol and the tertiary amine. A more intense signal is also observed at 1.6 V attributed to the oxidation of the pyridine moiety of the ligand. Upon the addition of manganese salt and base a new one-electron irreversible anodic process appears at $E^p = 0.53$ V vs. SCE attributed to the Mn^{III} to Mn^{IV} oxidation. Concomitantly a well defined anodic irreversible wave appears at −1.48 V vs. SCE corresponding to the reduction of the protonated lutidine [32], thus confirming that H_3L has been deprotonated. The Mn^{III}/Mn^{IV} oxidation potential value ($E^p = 0.53$ V vs. SCE) is 100 mV higher than the one reported for the mononuclear Mn^{III} complex with a N_2O_3 coordination sphere, Mn(salbutO) [12]. This difference is attributed to the lower stabilization of Mn^{III} oxidation state with amine in comparison to the one with imine moieties. The CH_3CN solution of MnL prepared from a solid sample of the complex also shows the oxidation wave at $E^p = 0.53$ V (Fig. S8).

3.3. SOD activity

The activity of complex MnL toward superoxide in aqueous buffer was evaluated using the NBT assay, which is based on kinetic competition between NBT and the complex for reacting with $O_2^{\bullet-}$. In this assay SOD activity is inversely related to the amount of formazan, the purple product formed by the reaction of NBT with superoxide, observed at 560 nm. Addition of the complex to the reaction mixture inhibits the reduction of NBT, as shown in Fig. 6. Inhibition percentages were measured for several complex concentrations and the IC_{50} value, graphically evaluated, was 1.26 μM. On the basis of competition with NBT, at 50% inhibition of the rates of the reactions of $O_2^{\bullet-}$ with NBT and the mimic are equal, k_{cat} [catalyst] = k_{NBT} [NBT], where k_{NBT} (pH = 7.8) = 5.94×10^4 M^{-1} s^{-1} [33,34]. Hence, the catalytic rate constant, $k_{cat} = k_{NBT}$ [NBT] / IC_{50}, was calculated: $k_{cat} = 1.7 \times 10^6$ M^{-1} s^{-1}. These values are independent of the detector concentration and appropriate for comparison with literature data.

The SOD-like activity of complex MnL is in the range of other MnSOD mimics with open chain ligands (Table 1) [7–13,33,35], which clearly indicates that this complex can be used as $O_2^{\bullet-}$ scavenger. The low anodic potential of the Mn^{III}/Mn^{IV} couple of MnL (although measured in CH_3CN) may account for efficient redox cycling of $O_2^{\bullet-}$ employing $Mn^{III/IV}$ oxidation states, such as observed for Mn(salbutO), which shows similar SOD activity and Mn^{III}/Mn^{IV} oxidation at 430 mV (vs.

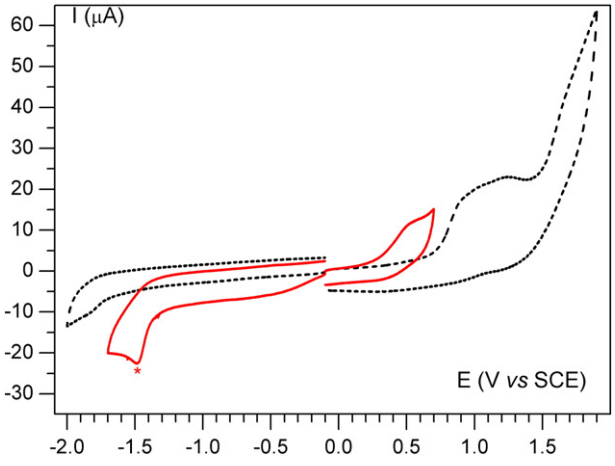

Fig. 5. Cyclic voltammogram of H_3L, 1 mM in CH_3CN + $TBAPF_6$, 0.1 M (black dashed line) and in presence of 1 mM of $[Mn(H_2O)_6](ClO_4)_2$ and 1 mM lutidine (red, solid trace). Conditions: Glassy carbon electrode, $T = 293$ K, v = 0.1 $V.s^{-1}$. * indicates reduction of lutidinium.

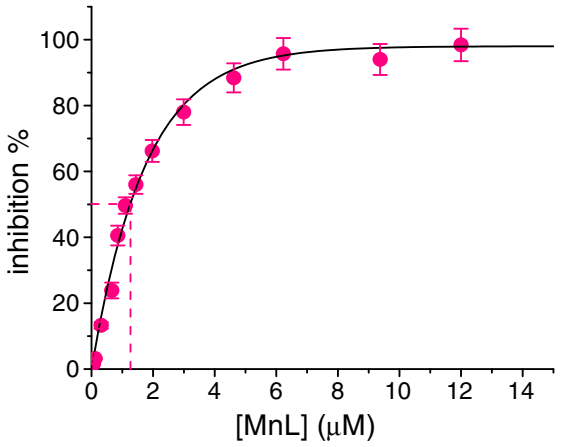

Fig. 6. SOD activity of MnL in the riboflavin-methionine-NBT assay.

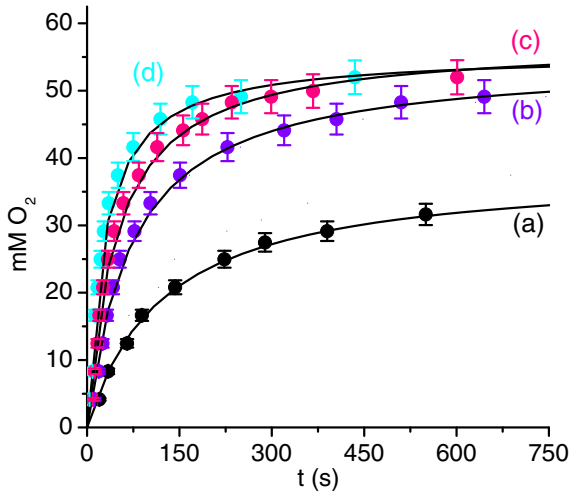

Fig. 7. Oxygen evolved from a mixture of H_2O_2 (100 mM) and (a) 0.33, (b) 0.62 (c) 0.89 and (d) 1.12 mM MnL in 5 mL of CH_3CN. $T = 293$ K. Experimental data are the mean of at least three determinations.

SCE) [12]. The other MnSOD mimics shown in Table 1, either tetragonal Mn complexes (Mn-salen, Mn-salpn, Mn-salpnOH) [7–10,36] or Mn complexes with N-rich first coordination sphere (MnL^{1-3}, $Mn(BMPG)^+$, $Mn(PI)_2^+$, MnImtacn, MnBimtacn) [13,14,33,35], show Mn^{III}/Mn^{II} reduction potential within the range from −0.4 V ($O_{2(aq)}/\ O_2^{\bullet-}$) to 0.65 V ($O_2^{\bullet-}/H_2O_2$) vs. SCE, thus cycling between Mn^{II}/Mn^{III} oxidation states. The present result reinforces the idea that SOD mimics employ the metal-centered redox couple closest to the midpoint between the oxidation and reduction of $O_2^{\bullet-}$, either Mn^{II}/Mn^{III} or Mn^{III}/Mn^{IV}, to be an efficient scavenger.

3.4. Catalase activity of MnL

The ability of MnL to catalyze disproportionation of H_2O_2 into O_2 and H_2O was tested in CH_3CN by volumetric measurement of evolved O_2. Addition of H_2O_2 to a solution of the catalyst causes an immediate vigorous evolution of O_2 coupled to color change from brown to yellowish-brown. The O_2 evolution was evaluated in excess of H_2O_2 and at constant temperature, and the dependence of the reaction rate with [catalyst] and $[H_2O_2]_0$ was determined by varying [catalyst] at fixed $[H_2O_2]_0$ (Fig. 7), and varying the $[H_2O_2]_0$ at constant [catalyst] (Fig. 8). Analogous kinetic results were obtained when H_2O_2 was added to the in situ generated complex (prepared as described in Section 3.2. for the electrochemical measurements).

At constant $[H_2O_2]_0 = 100$ mM, the reaction exhibits second-order kinetics on [catalyst], and experimental data could be fitted to the $r_i = k\,[\text{catalyst}]^2$ equation (Fig. 9(a)), from which the second-order rate constant $k = 2.17(2)\ mM^{-1}\ s^{-1}$ was obtained. At fixed [catalyst] = 0.6 mM, initial rates show a good linear dependence with $[H_2O_2]_0$ indicating that the reaction is first-order on $[H_2O_2]$. The third-order catalytic constant $k_{cat} = 0.0221(2)\ mM^{-2}\ s^{-1}$ was obtained from the slope of the plot of $r_i/[cat]^2$ vs. $[H_2O_2]_0$ (Fig. 9(b)).

Table 1
SOD activity of MnL and other MnSOD models.

Complex	SOD activity		SOD test	E (V) vs. SCE	Ref.
	IC_{50} (μM)	$10^{-6}\ k_{McCF}$ ($M^{-1}\ s^{-1}$)			
MnL	1.26	1.7	pH 7.8[a]	+0.53 (E^p)	This work
Mn(X-salen)(OAc)	0.3–3	–	pH 7.8[b]	−0.2–+0.1[d]	[7,8,36]
Mn(3-OMe-salenR)(OAc)	0.044–0.146	–	pH 7.4[c]	−0.22 - -0.17[d]	[9]
Mn(X-salpn)S_2	0.77	3.6	pH 7.8[a]	−0.07[d]	[10]
Mn(X-salpnOH)	1.14	2.4	pH 7.8[a]	−0.04[d]	[10]
Mn(salbutO)N_3	1.43	1.91	pH 7.8[a]	+0.43[e]	[12]
$MnL^1(OTf)_2$	1.51	4.2	pH 7.4[b]	ND	[13]
$MnL^2(OTf)_2$	1.41	3.9			
Mn(Imtacn)Cl_2	8.33	0.52	pH 7.8[a]	+0.15[d]	[14]
Mn(Bimtacn)$Cl\cdot ClO_4$	5.36	0.33		+0.52[d]	
MnL^3	0.81	7.0	pH 7.8[c]	+0.2[d]	[35]
$Mn(BMPG)^+$	1.2	4.8	pH 7.8[c]	+0.44[d]	[33]
$Mn(PI)_2^+$	0.8	6.6		+0.34[d]	

[a]Riboflavin–methionine–NBT assay.
[b]Xanthine–Xanthine Oxidase–NBT assay.
[c]Xanthine-Xanthine oxidase-cytochrome *c* assay.
[d]Mn^{II}/Mn^{III} couple.
[e]Mn^{III}/Mn^{IV} couple.
X = phenyl-ring substituent.
S = solvent or labile ligand.
R = cyclopentane-fused with ureido or acid–base catalyst auxiliary.
Salpn: 1,3-bis(salicylidenamino)propane.
salpnOH = 1,3-bis(salicylidenamino)propan-2-ol.
salbutOH = 1,4-bis(salicylidenamino)butan-2-ol.
L^1 = 2,6-Bis[(*N*-methyl(2-pyridylmethyl)amino)methyl]pyridine.
L^2 = 2,6-bis[((2-pyridylmethyl)oxy)methyl]pyridine.
L^3H = *N*-(2-hydroxybenzyl)-*N*,*N*′-bis[2-(*N*-methylimidazolyl)methyl]ethane-1,2-diamine.
BMPG = *N*,*N*-bis[(6-methyl-2-pyridyl)methyl]glycinate.
PI^- = 2-{[(1-methyl-2-imidazolyl)methyl]amino}phenolate.
Imtacn = 1-(benzimidazol-2-ylmethyl)-1,4,7-triazacyclononane.
Bimtacn = 1,4-bis(benzimidazol-2-ylmethyl)-1,4,7-triazacyclononane.
Schemes of the ligands are given in the SI.
ND = not determined.

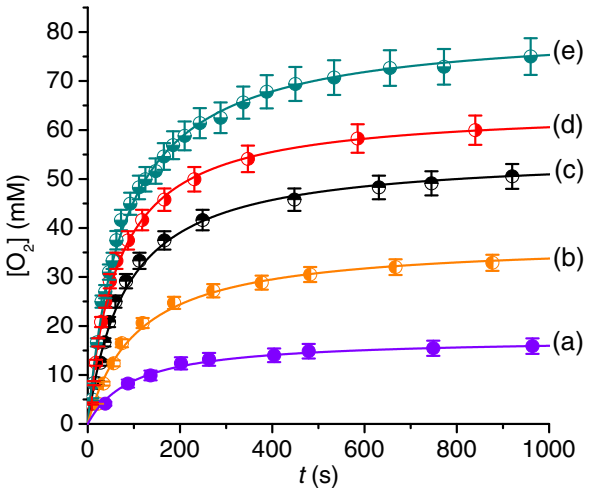

Fig. 8. Oxygen evolved from a mixture of MnL (0.6 mM) and (a) 50, (b) 100, (c) 165, (d) 250 and (e) 330 equiv. of H_2O_2, in 5 mL of CH_3CN. $T = 293$ K. Experimental data are the mean of at least three determinations.

In this solvent, the complex converts more than 300 equiv of H_2O_2 to O_2. However, although successive additions of excess H_2O_2 to the catalyst solution yield the stoichiometric amount of O_2, the initial rate of H_2O_2 dismutation gradually decreases after each new addition (Fig. 10(a)). UV–vis spectra taken at the end of O_2 evolution also show that the initial spectral pattern of the complex is retained, but the intensity of the LMCT absorption bands decreases (Fig. 10(b)). After the third 100:1 excess of H_2O_2 was added to the solution of catalyst, the intensity of LMCT bands decreased down to 55% of initial value, probably as a result of the gradual loss of catalyst. The observation of Mn^{2+} in the EPR spectra of the reaction mixtures (inset in Fig. 9(b)) also evidences partial loss of catalyst by metal dissociation.

Second-order dependence of the reaction on [catalyst] and first-order on $[H_2O_2]$, imply the involvement of two molecules of the starting complex and one molecule of H_2O_2 at (or before) the slow step of the catalytic cycle. Two paths involving two molecules of the starting complex are shown in Scheme 2. In mechanism (a), it is proposed that the catalytic cycle initiates upon binding of peroxide to the starting complex through a ligand shift with the endogenous alkoxo-group acting as internal base to assist deprotonation of a terminally bound HO_2^-. Reaction with a second complex molecule in the slow reductive half-reaction (turnover-limiting step) yields the oxidized active form of catalyst $[(HL)Mn(O)]_2$ or 2 [(HL)Mn(O)] coupled to the peroxide two-electron reduction, without change in the total formal charge of the catalyst. The so-formed $Mn^{IV}{}_2$ (or 2 Mn^{IV}) complex reacts with another H_2O_2 molecule in the fast oxidative half-reaction to yield O_2 and restore the reduced active form of the catalyst: $[(HL)Mn^{III}(OH)]$, thus closing the cycle.

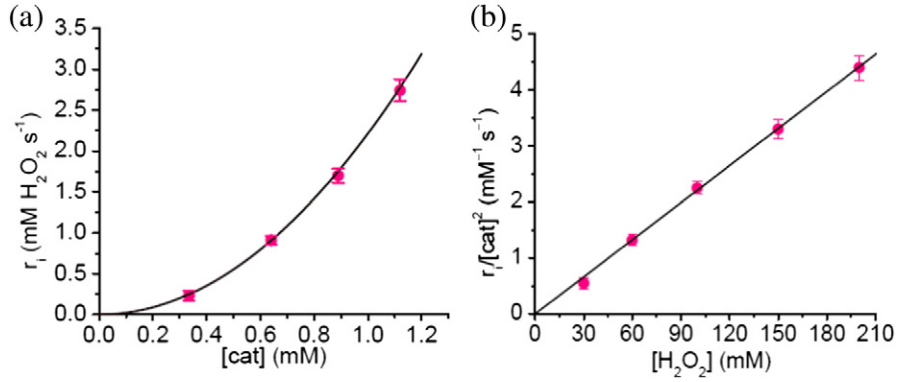

Fig. 9. Effect of (a) [catalyst] and (b) $[H_2O_2]$, on the initial rate of H_2O_2 disproportionation by MnL, at 293 K, in CH_3CN. Solid line corresponds to the least-square fit of experimental data to rate equation.

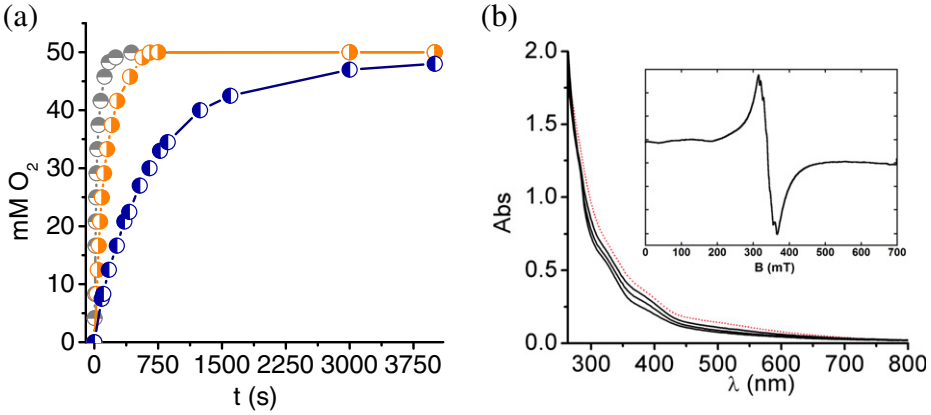

Fig. 10. (a) Time dependence of O_2 evolution after three successive additions of 100 equiv H_2O_2 over 5 mL of a 1.1 mM solution of MnL in CH_3CN. (b) Electronic spectra in CH_3CN, registered before (pink dashed line) and after three successive additions of 100 equiv of H_2O_2 (black solid lines) to a 0.123 mM solution of MnL. $T = 293$ K, l = 1 cm. Inset: EPR spectrum of 1 mM MnL + 100 equiv. H_2O_2 in CH_3CN, incubated at room temperature overnight. $\nu = 9.5$ GHz, $T = 100$ K.

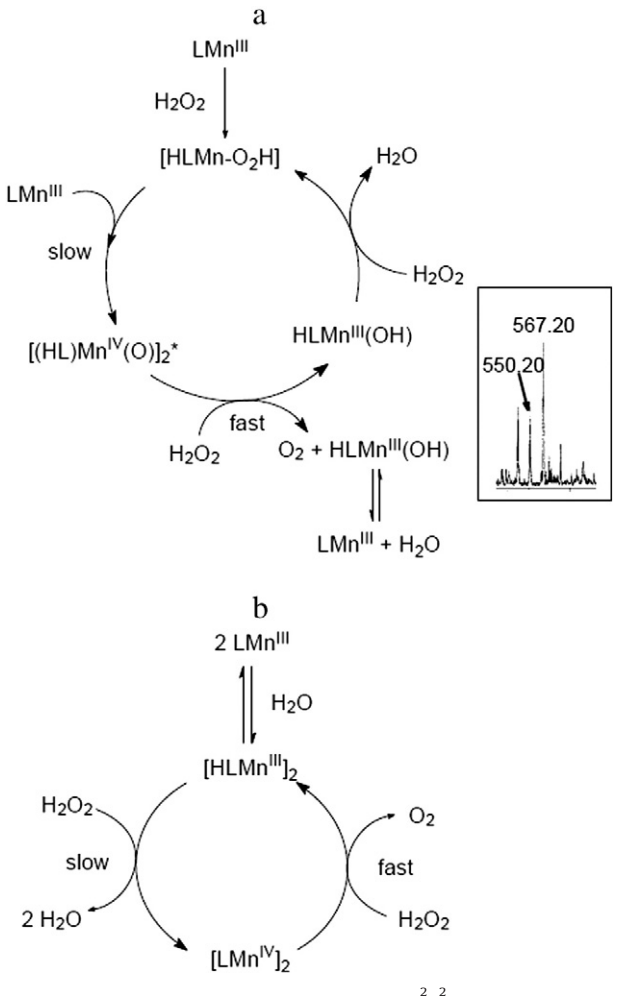

Scheme 2. Alternative paths for the reaction of MnL with H_2O_2. Inset: ESI-mass spectrum of a MnL/H_2O_2 reaction mixture in CH_3CN.

In a mechanism such as (b), water-induced dimerization occurs before the complex enters the catalytic cycle of H_2O_2 disproportionation, which takes place between two dimeric active forms of the catalyst. In both mechanisms, the catalytic cycle is proposed to run between Mn^{III}_2 and Mn^{IV}_2 oxidation states, in agreement with the low redox potential observed for the Mn^{III}/Mn^{IV} couple. Besides, if Mn^{III} is the major species in the mixture, the oxidation of the catalyst must occur in the slow redox step, which is consistent with the retention of the spectral pattern in the electronic spectra registered during the reaction. Although kinetics does not distinguish between the two paths shown in Scheme 2, the presence of the peak at *m/z* 567.2 –which corresponds to the [(HL)Mn(OH)]—, in the ESI-mass spectra registered after addition of H_2O_2 to the complex in CH_3CN (inset in Scheme 2) and the absence of the peak belonging to the dimer in the ESI-M spectra of the reaction mixture, support mechanism (a) for CAT activity of complex MnL.

In Table 2, initial rate and maximal turnover number of H_2O_2 disproportionation by MnL is compared to other mononuclear Mn complexes.

It can be seen that, independently from the solvent, the present complex reacts at similar rate as mononuclear Mn complexes with one or two labile coordination positions on the Mn ion [7–15,17–19]. Catalysts evaluated in aqueous media require the addition of exogenous base to show activity. Thus, Mn(chedam)(bipy)(H_2O) is inactive in water, but exhibits high turnover numbers upon addition of imidazole [19]. In the case of Mn–Schiff-base complexes, even in the presence of base, exhibit maximal turnover numbers much lower than complexes tested in non-aqueous solvents [7–10]. MnL and $Mn(Y\text{-}Ind)_2$ [23], the two complexes with six coordination sites of Mn occupied by donor sites of the ligand, are able to disproportionate H_2O_2 in non-aqueous solvents. MnL (coordination sphere: $Mn–N_3O_3$) reacts faster than $Mn(Y\text{-}Ind)_2$ (coordination sphere: $Mn–N_6$), probably because the central alcohol group in MnL is better to act as an internal base assisting H_2O_2 dismutation, such as proposed in Scheme 2(a). In line with this, MnL reacts faster than complexes of pentadentate N_5-donor ligands [14], in the same solvent.

4. Conclusions

Hexadentate N_3O_3-ligand L^{3-} affords MnL, a complex able to disproportionate both H_2O_2 and $O_2^{\bullet-}$ in CH_3CN. Given the six coordination sites of Mn are occupied by donor sites of the ligand, initial binding to the substrate must occur through ligand shift with the ligand acting as internal base to assist substrate deprotonation coupled to the redox reaction. The accessibility of the Mn^{IV} state suggests that this complex employs a high-valent catalytic cycle to decompose either $O_2^{\bullet-}$ or H_2O_2. The CAT-like activity of MnL, although lower than the observed for dinuclear or dimeric catalysts [6,16], is in the same order as mononuclear Mn complexes with one or two labile coordination positions on the metal ion. Disproportionation of H_2O_2 occurs with second-order kinetics on catalyst, thus evidencing the requirement of two molecules of catalyst in the slow redox half-reaction, a fact also observed for other complexes that employ high-valent catalytic cycle but are active only if a base is present [37]. Further catalytic studies of new "congeners" of MnL are currently underway in our laboratories.

Abbreviations

Bimtacn	1,4-bis(benzimidazol-2-ylmethyl)-1,4,7-triazacyclononane
BMPG	*N*,*N*-bis[(6-methyl-2-pyridyl)methyl]glycinate
Bipy	bipyridine
CAT	catalase
Chedam	4-hydroxypyridine-2,6-dicarboxylic acid
2-CH_2OHpy	2-hydroxymethylpyridine
H_3L	1-[N-(2-pyridylmethyl),*N*-(2-hydroxybenzyl)amino]-3-[*N*′-(2-hydroxybenzyl), *N*′-(4-methylbenzyl)amino]propan-2-ol
E^p	anodic peak potential
ESI-MS	electrospray ionization mass spectrometry
HSQC	heteronuclear Single Quantum Coherence
IC_{50}	concentration for 50% inhibition
Imtacn	1-(benzimidazol-2-ylmethyl)-1,4,7-triazacyclononane
IndH	1,3-bis(2-pyridylimino)isoindoline
L^1	2,6-Bis[(*N*-methyl(2-pyridylmethyl)amino)methyl]pyridine
L^2	2,6-bis[((2-pyridylmethyl)oxy)methyl]pyridine
L^3H	*N*-(2-hydroxybenzyl)-*N*,*N*′-bis[2-(*N*-methylimidazolyl)methyl]ethane-1,2-diamine
LMCT	ligand-to-metal charge transfer
PI^-	2-{[(1-methyl-2-imidazolyl)methyl]amino}phenolate
MnCAT	manganese catalase
MnSOD	manganese superoxide dismutase
NBT	nitro blue tetrazolium
r_i	initial rate
ROS	reactive oxygen species
salbutOH	1,4-bis(salicylidenamino)butan-2-ol
Salpn	1,3-bis(salicylidenamino)propane
salpnOH	1,3-bis(salicylidenamino)propan-2-ol
SCE	saturated calomel electrode
SOD	superoxide dismutase
TMS	tetramethylsilane

Acknowledgments

We thank the National University of Rosario and CONICET for financial support (PIP 0335) and CONICET-CNRS for a bilateral agreement (Res. 991/2013).

Table 2
CAT activity of MnL and other mononuclear Mn complexes.

Complex	CAT activity		Ligand donor Sites	Solvent	Ref.
	r_i[a] (mmol O_2 mmol cat^{-1} min^{-1})	TON[b]			
MnL	13.2[c]	>300	N_3O_3	CH_3CN	This work
Mn(X-salen)(OAc)	11–24	2.5–8.4	N_2O_2	H_2O, pH 8.1	[7,8]
Mn(3-OMe-salenR)(OAc)	8–29	4–17	N_3O_2	H_2O, pH 7.4	[9]
Mn(X-salpn)S_2·NO_3	–	16–26	N_2O_2	CH_3OH	[10,11]
Mn(X-salpnOH)	3.6	0.5	N_2O_2	H_2O, pH 8.1	[7,10]
Mn(salbutO)N_3	3.4	1200	N_2O_3	DMF	[12]
$MnL^1(OTf)_2$	0.16	17	N_5	CH_3CN	[13]
$MnL^2(OTf)_2$	0.1	24			
Mn(Imtacn)Cl_2	6.7	600	N_4	CH_3OH /H_2O + 6 eq NaOH	[14]
Mn(Bimtacn)Cl·ClO_4	1.2	600	N_5		
$Mn(L^3)^+$	3.5	4	N_4O	H_2O, pH 7	[15]
Mn(IndH)Cl_2	23	–	N_3	H_2O, pH 9.5	[16]
Mn(2-CH_2OHpy)(SO_4)(H_2O)	3.0×10^{-5}	320[d]	NO	H_2O	[17]
Mn(chedam)(bipy)(H_2O)	0.7	5000	NO_2,N_2	H_2O + Im	[18]
Mn(Y-Ind)$_2$	1.24–1.7	–	N_3	DMF	[22]

[a] r_i values were calculated from reported kinetic data.
[catalyst] = 10 μM; [H_2O_2] = 10 mM.
[b] Total mmol O_2/mmol catalyst.
[c] r_i / $[MnL]^2$.
[d] Five days.
X = phenyl-ring substituent.
S = solvent or labile ligand.
R = cyclopentane-fused with ureido or acid–base catalyst auxiliary.
Salpn, salpnOH, salbutOH, L^1, L^2, Imtacn, Bimtacn.
L^3 as in Table 1.
IndH = 1,3-bis(2-pyridylimino)isoindoline.
2-CH_2OHpy = 2-hydroxymethylpyridine.
Chedam = 4-hydroxypyridine-2,6-dicarboxylic acid.
Y-Ind = 1,3-bis(2′-pyridylimino)isoindoline, Y = H, 4-Me.
Schemes of the ligands are given in the SI.

Appendix A. Supplementary data

Supplementary data to this article can be found online at http://dx.doi.org/10.1016/j.jinorgbio.2015.02.012.

References

[1] A. Sigel, H. Sigel (Eds.), Metal Ions in Biological Systems Vol 37: Manganese and its Role in Biological Processes, Marcel Dekker, New York, 2000.
[2] S. Signorella, C. Palopoli, V. Daier, G. Ledesma, in: R.H. Kretsinger, E.A. Permyakov, V.N. Uversky (Eds.), Encyclopedia of Metalloproteins, Springer, New York, 2013, pp. 1283–1292.
[3] W.C. Stallings, K.A. Pattridge, R.A. Strong, M.L. Ludwig, J. Biol. Chem. 260 (1985) 16424–16432.
[4] Y. Sheng, I.A. Abreu, D.E. Cabelli, M.J. Maroney, A.-F. Miller, M. Teixeira, J.S. Valentine, Chem. Rev. 114 (2014) 3854–3918.
[5] O. Iranzo, Bioorg. Chem. 39 (2011) 73–87.
[6] S. Signorella, C. Hureau, Coord. Chem. Rev. 256 (2012) 1229–1245.
[7] S.R. Doctrow, K. Huffman, C. Bucay Marcus, G. Tocco, E. Malfroy, C.A. Adinolfi, H. Kruk, K. Baker, N. Lazarowych, J. Mascarenhas, B. Malfroy, J. Med. Chem. 45 (2002) 4549–4558.
[8] M. Baudry, S. Etienne, A. Bruce, M. Palucki, E. Jacobsen, B. Malfroy, Biochem. Biophys. Res. Commun. 192 (1993) 964–968.
[9] Y. Noritake, N. Umezawa, N. Kato, T. Higuchi, Inorg. Chem. 52 (2013) 3653–3662.
[10] D. Moreno, V. Daier, C. Palopoli, J.-P. Tuchagues, S. Signorella, J. Inorg. Biochem. 104 (2010) 496–502.
[11] M.A. Vázquez-Fernández, M.R. Bermejo, M.I. Fernández-García, G. González-Riopedre, M.J. Rodríguez-Doutón, M. Maneiro, J. Inorg. Biochem. 105 (2011) 1538–1547.
[12] V. Daier, D. Moreno, C. Duhayon, J.-P. Tuchagues, S. Signorella, Eur. J. Inorg. Chem. (2010) 965–974.
[13] M. Grau, F. Rigodanza, A.J.P. White, A. Soraru, M. Carraro, M. Bonchio, G.J.P. Britovsek, Chem. Commun. 50 (2014) 4607–4609.
[14] Q.X. Li, Q.-H. Luo, Y.Z. Li, Z.Q. Pan, M.C. Shen, Eur. J. Inorg. Chem. (2004) 4447–4456.
[15] A.S. Bernard, C. Giroud, H.Y.V. Ching, A. Meunier, V. Ambike, C. Amatore, M.G. Collignon, F. Lemaître, C. Policar, Dalton Trans. 41 (2012) 6399–6403.
[16] A.J. Wu, J.E. Penner-Hahn, V.L. Pecoraro, Chem. Rev. 104 (2004) 903–938.
[17] J. Kaizer, T. Csay, P. Kovari, G. Speier, L. Parkanyi, J. Mol. Catal. A Chem. 280 (2008) 203–209.
[18] M. Zienkiewicz, J. Szlachetko, C. Lothschütz, M. Hodorowicz, A. Jabłońska-Wawrzycka, J. Sá, B. Barszcz, Dalton Trans. 42 (2013) 7761–7767.
[19] M. Devereux, M. McCann, V. Leon, V. McKee, R.J. Ball, Polyhedron 21 (2002) 1063–1071.
[20] Y. Watanabe, A. Namba, N. Umezawa, M. Kawahata, K. Yamaguchi, T. Higuchi, Chem. Commun. (2006) 4958–4960.
[21] J.I. Yang, D.G. Nocera, J. Am. Chem. Soc. 129 (2007) 8192–8198.
[22] M. Maneiro, M.R. Bermejo, M.I. Fernández, E. Gómez-Fórneas, A.M. González-Noya, A.M. Tyryshkin, New J. Chem. 27 (2003) 727–733.
[23] J. Kaizer, G. Baráth, G. Speier, M. Reglier, M. Giorgi, Inorg. Chem. Commun. 10 (2007) 292–294.
[24] G. Ledesma, S. Signorella, Tetrahedron Lett. 53 (2012) 5699–5702.
[25] C. Beauchamps, I. Fridovich, Anal. Biochem. 44 (1971) 276–287.
[26] G.N. Ledesma, E. Anxolabéhère-Mallart, E. Rivière, S. Mallet-Ladeira, C. Hureau, S.R. Signorella, Inorg. Chem. 53 (2014) 2545–2553.
[27] M. Hirotsu, M. Kojima, W. Mori, Y. Yoshikawa, Bull. Chem. Soc. Jpn. 71 (1998) 2873–2884.
[28] H. Biava, C. Palopoli, C. Duhayon, J.P. Tuchagues, S. Signorella, Inorg. Chem. 48 (2009) 3205–3214.
[29] L. Dubois, D.F. Xiang, S.S. Tan, J. Pecaut, P. Jones, S. Baudron, L. Le Pape, J.M. Latour, C. Baffer, S. Chardon-Noblat, M.N. Collomb, A. Deronzier, Inorg. Chem. 42 (2003) 750–760.
[30] C. Hureau, L. Sabater, F. Gonnet, G. Blain, J. Sainton, E. Anxolabéhère-Mallart, Inorg. Chim. Acta 359 (2006) 339–345.
[31] D.W. Wright, H.J. Mok, C.E. Dubé, W.H. Armstrong, Inorg. Chem. 37 (1998) 3714–3718.
[32] C. Hureau, G. Blondin, M.-F. Charlot, C. Philouze, M. Nierlich, M. Césario, E. Anxolabéhère-Mallart, Inorg. Chem. 44 (2005) 3669–3683.
[33] S. Durot, C. Policar, F. Cisnetti, F. Lambert, J.-P. Renault, G. Pelosi, G. Blain, H. Korri-Youssoufi, J.-P. Mahy, Eur. J. Inorg. Chem. (2005) 3513–3523.
[34] Z.R. Liao, X.F. Zheng, B.S. Luo, L.R. Shen, D.F. Li, H.L. Liu, W. Zhao, Polyhedron 20 (2001) 2813–2821.
[35] F. Cisnetti, A.-S. Lefèvre, R. Guillot, F. Lambert, G. Blain, E. Anxolabéhère-Mallart, C. Policar, Eur. J. Inorg. Chem. (2007) 4472–4480.
[36] M.R. Bermejo, A. Castiñeiras, J.C. Garcia-Monteagudo, M. Rey, A. Sousa, M. Watkinson, C.A. McAuliffe, R.G. Pritchard, R.L. Beddoes, J. Chem. Soc. Dalton Trans. (1996) 2935–2944.
[37] E.J. Larson, P.J. Riggs, J.E. Penner-Hahn, V.L. Pecoraro, J. Chem. Soc. Chem. Commun. (1992) 102–103.